UNCLASSIFIED

AD 274 098

Reproduced
by the

ARMED SERVICES TECHNICAL INFORMATION AGENCY
ARLINGTON HALL STATION
ARLINGTON 12, VIRGINIA

UNCLASSIFIED

NOTICE: When government or other drawings, specifications or other data are used for any purpose other than in connection with a definitely related government procurement operation, the U. S. Government thereby incurs no responsibility, nor any obligation whatsoever; and the fact that the Government may have formulated, furnished, or in any way supplied the said drawings, specifications, or other data is not to be regarded by implication or otherwise as in any manner licensing the holder or any other person or corporation, or conveying any rights or permission to manufacture, use or sell any patented invention that may in any way be related thereto.

CATALOGED BY ASTIA
AS AD NO. 274058

Office of Naval Research
Department of the Navy
Contract Nonr-220(28)

AN ANALYSIS OF ECHOES FROM A SOLID ELASTIC SPHERE IN WATER

by
Robert Hicking

1 x-3 NOX

Engineering Division
CALIFORNIA INSTITUTE OF TECHNOLOGY
Pasadena, California

Report No. 85-20
March, 1962

Approved by:
M. S. Plesset

Office of Naval Research
Department of the Navy
Contract Nonr-220(28)

AN ANALYSIS OF ECHOES FROM A SOLID ELASTIC SPHERE IN WATER

Robert Hickling

Reproduction in whole or in part is permitted for any purpose of the United States Government

Engineering Division
California Institute of Technology
Pasadena, California

Report No. 85-20
March, 1962

Approved by:
M. S. Plesset

AN ANALYSIS OF ECHOES FROM A SOLID ELASTIC SPHERE IN WATER

Robert Hickling

California Institute of Technology
Pasadena, California

Abstract

It is well-known in sonar work that the pulse form of a direct echo from a target bears little relation to the form of the original signal. This is true even for regularly shaped bodies, such as a sphere. In this paper, the case of a homogeneous elastic sphere in water is examined theoretically and it is shown in comparison with experimental results, that the observed effects originate from vibrations induced in the sphere by the incident sound. Calculated results are presented for a variety of solid materials and it seems that echo forms could possibly provide information about the size and constitution of a sonar target.

1. Introduction

It is well-known in sonar work that the pulse form of the direct echo returned by a stationary insonified target in water is usually quite different from that of the original signal sent out by the transducer. This effect can be observed even when the target has a regular shape as in the case of a sphere. In the experiments which have been made, the incident sound has consisted of single frequency, constant amplitude pulses of various lengths, and the echo pulse generally appears in the form of multiple echoes of the original pulse; i.e. compared to the original pulse, the echo is generally longer and subject to amplitude modulation. Presumably there are also differences in frequency content, but there does not appear to be any quantitative data available on the subject.

If the body has an irregular shape it is possible to suppose that this effect is due to echoes returned by the individual irregularities. However in the case of regularly shaped bodies with no abrupt changes in curvature, such an explanation cannot be used. In this event it would seem reasonable to suppose that the distortion in the echo is caused either by diffraction or by vibrations occurring within the solid material of the target or by both. The frequencies used in sonar usually preclude the influence of diffraction, so that the observed effects would appear to be due mainly to vibrations in the solid. Since the density of any solid does not differ from that of water by much more than a factor of eight, it seems quite possible for the incident sound to cause vibrations in the solid material of the target. In air the corresponding density ratio would be of the order of 10^4 so that a target would react more like a rigid body,

with a consequent diminution in echo distortion.

It is the purpose of this paper to test the validity of this hypothesis in the case of a homogeneous solid sphere supporting shear and compressional waves. Suitable experimental data[1] has recently become available and this is compared with calculated results based on known formal solutions[2],[3]. These results were obtained using a high speed computer. Previous calculations have been made for fluid[4] and rigid[5] spheres.

2. Formulation of the Problem

The coordinate system for the sphere is shown in Fig. 1 where the relationship between the cartesian and spherical polar coordinates is

$$x = r \sin\theta \cos\phi \ ,$$
$$y = r \sin\theta \sin\phi \ ,$$
$$z = r \cos\theta \ . \qquad (1)$$

The sphere is assumed to consist of solid isotropic material supporting both compressional and shear waves. The displacement vector $\vec{u}$ can be expressed using the vector and scalar potentials $\vec{A}$ and ψ as follows[6]

---

[1] L.D. Hampton and C.M. McKinney; J.A.S.A., 33, 5, 1961, p. 664.

[2] J. J. Faran; J.A.S.A., 23, 4, 1951, p. 405.

[3] P. M. Morse and H. Feshbach; "Methods of Theoretical Physics" (McGraw-Hill Book Company, New York, 1953) Vol. II, p. 1483.

[4] V. C. Anderson; J.A.S.A. 22, 4, 1950, p. 426.

[5] H. Stenzel; Leitfaden zur Berechnung von Schallvorgagen, Julius Springer, Berlin, 1939.

[6] Morse and Feshbach p. 142

$$\vec{u} = -\nabla\psi + \nabla\times\vec{A} \quad , \tag{2}$$

where

$$\nabla^2\psi = (1/c_1^2)\,\partial^2\psi/\partial t^2 \quad , \tag{3}$$

$$\nabla^2\vec{A} = (1/c_2^2)\,\partial^2\vec{A}/\partial t^2 \quad , \tag{4}$$

describe the motion of the compressional and shear waves respectively, c_1 and c_2 are the compressional and shear wave velocities defined by

$$c_1 = [E(1-\sigma)/\rho_1(1+\sigma)(1-2\sigma)]^{\frac{1}{2}}$$

$$c_2 = [E/2\rho_1(1+\sigma)]^{\frac{1}{2}} \quad , \tag{5}$$

where E, ρ_1, σ are the Young's modulus, density and Poisson's ratio of the solid material of the sphere.

Outside the sphere there is a limitless fluid of density ρ and sound velocity c in which there is a continuous train of waves emanating from a point source situated on the z axis at $r = r_o$, $\theta = \pi$. The time dependence of these waves is of the form $\exp(-i\omega t)$ from which the wave number k in the fluid is obtained by means of the relation

$$k = \omega/c = 2\pi/\lambda$$

where λ is the wave length. Similar relations

$$k_1 = \omega/c_1 \quad ; \quad k_2 = \omega/c_2$$

hold for the compressional and shear waves in the solid. The waves emanating from the point source can be expressed[7]

---

[7] ibid p. 1466

$$p_i = P_o \exp(ikD)/D$$

$$= ik P_o \sum_{n=o}^{\infty} (2n+1)(-1)^n P_n(\cos\theta) j_n(kr) h_n(kr_o) \qquad 0 < r < r_o \tag{6}$$

where

$$D = [r_o^2 + 2r\, r_o \cos\theta + r^2]^{\frac{1}{2}}$$

and the P_n are Legendre polynomials, and the j_n, h_n are spherical Bessel functions[8]. Plane waves incident on the sphere are obtained by making r_o go to infinity. Using the two limits

$$\exp(ikD)/D \longrightarrow \exp(ik\, r_o) \exp(ik\, r \cos\theta)/r_o$$

$$h_n(kr_o) \longrightarrow i^{-(n+1)} \exp(ik\, r_o)/kr_o \tag{7}$$

and removing the common factor $\exp(ik\, r_o)/r_o$ gives

$$p_i = P_o \exp(ikr \cos\theta)$$

$$= P_o \sum_{n=o}^{\infty} (2n+1) i^n P_n(\cos\theta) j_n(kr) \quad . \tag{8}$$

The above waves, p_i, incident on the sphere result in scattered waves in the fluid which will be of the form

$$p_s = P_o \sum_{n=o}^{\infty} c_n h_n(kr) P_n(\cos\theta) \tag{9}$$

---

[8] ibid p. 1325 and p. 1573

where the coefficients c_n have to be determined from the boundary conditions at the surface of the sphere. The appropriate conditions are:

(a) the pressure in the fluid is equal to the normal component of stress in the solid.

(b) the normal component of displacement of the fluid is equal to the normal component of displacement of the solid.

(c) the tangential components of shearing stress in the solid vanish at the surface.

These conditions can be expressed[9] in the relations

$$p_i + p_s + 2\rho_1 c_2^2 \left[\frac{\sigma}{(1-2\sigma)} \; \mathrm{div}\vec{u} + \frac{\partial u_r}{\partial r} \right] = 0 \tag{10}$$

$$u_{i,r} + u_{s,r} = u_r \tag{11}$$

and

$$\frac{\partial u_\theta}{\partial r} - \frac{u_\theta}{r} + \frac{1}{r} \frac{\partial u_r}{\partial \theta} = 0 \tag{12}$$

evaluated on the surface of the sphere at $r = a$. The displacement of the fluid in Eq. (11) is obtained from (6) and (9) by using

$$u_{i,r} + u_{s,r} = (1/\rho\omega^2) \; \partial(p_i + p_s)/\partial r \; . \tag{13}$$

Because of the symmetry of the incident waves, the component of displacement u_ϕ is taken to be zero and the ϕ component of the shearing stress can also be neglected. The only non-zero component of the vector

[9] ibid p. 142 and p. 116.

potential will be A_ϕ so that the potentials become

$$\psi = \sum_{n=o}^{\infty} a_n j_n(k_1 r) P_n(\cos\theta)$$

$$A_\phi = \sum_{n=o}^{\infty} b_n j_n(k_2 r) \frac{d}{d\theta} P_n(\cos\theta) \quad . \tag{14}$$

Using Eq. (2) these expansions can be inserted into the boundary conditions (10) - (12) and the coefficients of each normal mode equated. The coefficients c_n of the scattered waves in the fluid given by Eq. (9) can then be expressed as follows,

$$c_n = k(-1)^n(2n+1) h_n(kr_o) \sin\eta_n \exp(-i\eta_n) \tag{15}$$

where the angle η_n is given by

$$\tan\eta_n = -[j_n(x)F_n - j'_n(x)]/[n_n(x)F_n - n'_n(x)] \tag{16}$$

with

$$F_n = \frac{\rho}{\rho_1}\frac{x_2^2}{2} \frac{\dfrac{x_1 j_n'(x_1)}{x_1 j_n'(x_1) - j_n(x_1)} - \dfrac{2(n^2+n) j_n(x_2)}{(n^2+n-2) j_n(x_2) + x_2^2 j_n''(x_2)}}{\dfrac{x_1^2\left[\dfrac{\sigma}{1-2\sigma} j_n(x_1) - j_n''(x_1)\right]}{x_1 j'_n(x_1) - j_n(x_1)} - \dfrac{2(n^2+n)[j_n(x_2) - x_2 j_n'(x_2)]}{(n^2+n-2) j_n(x_2) + x_2^2 j_n''(x_2)}} \tag{17}$$

and

$$x = ka \quad ; \quad x_1 = k_1 a \quad ; \quad x_2 = k_2 a \quad .$$

The primes denote the derivative with respect to the argument. This result was first derived by Faran[2]. However there was an error in his presentation in which the factor $\sigma/(1-2\sigma)$ was misplaced. Finally it should be noted that the expression on the right hand side of Eq. (15) is of the form $f(x)/(f(x) + i\,g(x))$ where f, g are regular on the real axis. Hence there are no singularities when the argument is real, and the function can be integrated numerically in a straightforward manner. It also follows that the solution as presented is complete for all frequencies, i.e., the boundary conditions are fully satisfied by the shear and compressional waves postulated in Eq. (14).

Certain limiting cases are of interest. If $F_n \longrightarrow 0$, the solution would then apply to scattering by a rigid immovable sphere[10]. This would be the case for instance when the density of the solid was very much greater than that of the fluid. If $F_n \longrightarrow \infty$ the solution for scattering by a free surface sphere is obtained[11]. This corresponds to the condition where the normal stress at the surface of the sphere vanishes, which would result for example when the density of the material inside the sphere was very much less than that of the fluid.

From the above it follows that the echo returned by the solid sphere to the source is given by

---

[10] P. M. Morse; Vibration and Sound (McGraw-Hill Book Co. Inc. New York 1948) p. 354

[11] Morse and Feshbach p. 1483

$$p_e = \frac{P_o}{2r_o}\left[-2x_o \sum_{n=o}^{\infty} (2n+1)\sin\eta_n \exp(-i\eta_n) h_n^{\,2}(x_o)\right] \exp(-i\omega t)$$

$$= \frac{P_o}{2r_o} f(x, x_o, x_1, x_2) \exp(-ix\tau) \qquad (18)$$

where $x_o = kr_o = xR$, and $\tau = ct/a$. When the source is a large distance from the sphere

$$p_e = \frac{P_o a}{2r_o^{\,2}}\left[\frac{2}{x}\sum_{n=o}^{\infty} (-1)^n (2n+1)\sin\eta_n \exp(-i\eta_n)\right] \exp\left[ik(2r_o - ct)\right]$$

$$= \frac{P_o a}{2r_o^{\,2}} f_\infty(x, x_1, x_2) \exp\left[ix(2R-\tau)\right] . \qquad (19)$$

Removal of a factor $\exp(ik\,r_o)/r_o$ gives the solution for incident plane waves. Equations (18) and (19) can then be used to construct the echo due to a pressure pulse emanating from the source. Suppose the source emits a pulse of form $P_i(t)$. This can be expressed in terms of Fourier components as

$$P_i(t) = \frac{P_o c}{(2\pi)^{\frac{1}{2}} D}\int_{-\infty}^{\infty} g(k) \exp\left[ik(D-ct)\right] dk \qquad (20)$$

where D is as defined previously. The frequency spectrum $g(k)$ is found by taking the Fourier transform of the given pulse, i.e.,

$$g(k) = \frac{1}{(2\pi)^{\frac{1}{2}}}\int_{-\infty}^{\infty} P_i(t) \exp\left[-ik(D-ct)\right] dt \quad . \qquad (21)$$

With the new variable $x = ka$, the reflected pulse will be

$$P_e(\tau) = \frac{P_o c}{(2\pi)^{\frac{1}{2}} a r_o} \int_{-\infty}^{\infty} g(x)\, f(x, x_o, x_1, x_2) \exp(-ix\tau)\, dx \quad , \tag{22}$$

and when the point source moves to a large distance from the sphere

$$P_e(\tau) = \frac{P_o}{2(2\pi)^{\frac{1}{2}} r_o^2} \int_{-\infty}^{\infty} g(x)\, f_\infty(x, x_1, x_2) \exp[ix(2R-\tau)]\, dx \quad . \tag{23}$$

In general the echo given by (23) will differ in form from that of the incident pulse (20). Only for high frequencies in the special cases of a rigid and a free surface sphere will it be the same. It can be shown[12] that in the former case $f_\infty \longrightarrow \exp(-2ix)$ as x becomes large while for the free surface sphere $f_\infty \longrightarrow -\exp(-2ix)$. Hence if the frequencies contained in the pulse are in the high frequency range, Eq. (23) becomes

$$P_r(\tau) = \frac{P_o}{2(2\pi)^{\frac{1}{2}} r_o^2} \int_{-\infty}^{\infty} g(x) \exp[ix(2R-2-\tau)]\, dx$$

which means that the reflected pulse has the same form as the emitted pulse, but is returned time $2(r_o-a)/c$ later. This travel time indicates that the sound is reflected from a point source reflector at the point on the surface of the sphere nearest to the source of incident sound. A similar result holds for the free surface sphere except that the pulse is inverted.

---

[12] ibid p. 1554.

3. The Steady State Solutions

The steady state solutions given by the functions f in Eqs. (18), (19) were determined for a certain number of cases, the calculations being performed on a high speed computer. The results are shown Figs. 2-13.

The first results obtained were for the special cases of the rigid[10] and free surface[11] spheres for a distant point source of continuous waves. These are shown in Figs. 2(a), (b). The argument of the function f_∞ is presented divided by the variable $x = ka$. The results for the rigid sphere are in agreement with those of Stenzel[5]. For low frequencies the function is given by the initial terms in the series expansion which in the limit as x tends to zero are

$$\frac{2i}{x}\left[\frac{j_o'(x)}{h_o'(x)} - \frac{3j_1'(x)}{h_1'(x)}\right] \to 3x^2\left(1 - \frac{ix^3}{3}\right) ,$$

and

$$\frac{2i}{x}\,\frac{j_o(x)}{h_o(x)} \to 2(1-ix) ,$$

for the rigid and free surface spheres respectively. For the rigid sphere this represents the well-known condition of Rayleigh scattering where the scattered intensity is proportional to the fourth power of the frequency. For the free surface sphere the results are quite different. Not only does the scattered intensity reach maximum values at low frequencies, but the scattering is uniform in all directions. For high frequencies both solutions tend to form $\exp(-2ix)$, the free surface solution converging more rapidly than that of the rigid sphere. In the previous section, it was shown that this indicates that at high frequencies the sound is

mainly from a small area on the surface opposite the source and this would agree with physical intuition. At low frequencies the echo appears to come from the center of the rigid sphere and from a half radius position in the free surface sphere. As the frequency increases the apparent origin of the echo moves gradually towards the region on the surface opposite the source. This is shown in Fig. 2(b), where the phase of f_∞ divided by $x = ka$ represents distance along a radius inside the sphere. In the case of the rigid sphere these results can be readily understood by supposing that low frequency waves are intercepted by the entire cross section whereas high frequency waves behave as in geometrical optics and form a "bright spot" reflector on the surface opposite the source. With the free surface sphere the results at low frequencies are not so readily explainable except that as expected they differ from those for the rigid sphere.

The main body of results were derived for solid spheres supporting internal shear and compressional waves. The properties of the materials considered are given in Table I. The fluid outside the sphere was assumed to be water of density 1 gm/cc and compressional velocity 1,410 m/sec.

As an initial test of the programs, the results obtained by Faran[2] were recalculated. Since these were for $\sigma = \frac{1}{3}$ no error could result from the misplacing of the factor $\sigma/(1-2\sigma)$ mentioned in the previous section since this factor is unity. Good agreement was found.

Some of the results for the materials tested in Table I are given in detail in Figs. 3-11. As before these are for a distant source.

TABLE I[13]

Material	Density (gm/cc)	Poisson's Ratio σ	Compressional Velocity C_1 (m/sec)	Shear Velocity C_2 (m/sec)
Beryllium	1.87	0.05	12,890	8,880
Fused Silica	2.20	0.17	5,968	3,764
Heavy Silicate, Flint Glass	3.88	0.224	3,980	2,380
Armco Iron	7.70	0.29	5,960	3,240
Monel Metal	8.90	0.327	5,350	2,720
Aluminum	2.70	0.355	6,420	3,040
Yellow Brass	8.60	0.374	4,700	2,110
Lucite	1.18	0.40	2,680	1,100
Lead	11.34	0.43	1,960	690
Ice[14]	0.917	0.336	2,743	1,433

Generally the range of frequency was for values of ka up to 30, but for Armco Iron, ice and lucite the range extended to ka = 60, 20, 10 respectively. In addition to the pressure amplitude the phase variation is given for Armco Iron, and aluminum. In all cases the results begin at low frequencies as though the solid were a rigid body, changing in general

[13] American Inst. of Physics Handbook (McGraw-Hill Book Company, Inc. New York, 1957).

[14] D. L. Anderson; Trans. of Engin. Inst. of Canada, Vol. 2, pp. 116-122, 1958.

into a fairly regular series of peaks and minima as the frequency increases. With a rigid, incompressible material such as beryllium, the change from the rigid body solution is not very great. However, as the material becomes more compressible and pliant, the resonances tend to become more pronounced and more closely spaced. In the case of lucite and ice the resonances have become quite sharp and close together. This general trend was investigated by considering an average frequency interval between minima or between resonance peaks for each material. The results are shown in Fig. 12 plotted against the shear velocity c_2. Parameters other than c_2 were also considered such as Poisson's ratio σ, but with these the scatter of points was much greater. It appears therefore that this feature is most strongly dependent on the behavior of shear waves in the material. The successive peaks and minima which occur in the direct echo for a continuous frequency were shown by Faran[2] to be due to strong lobes of backscattered radiation forming and then splitting again into side lobes scattering in other directions. It seems therefore that shear waves play an important role in this process. Other general trends can be observed in Figs. 3 - 11. Peaks split off and merge as the properties of the material change, and as before it appears that the shear wave velocity is the dominant parameter. The density of the material seems to have a relatively unimportant effect in water. As the frequency increases there appears to be no tendency towards some constant limit as in the cases of the free surface and rigid spheres. The peaks seem to recur, but in an increasingly ragged form.

In the phase variations shown in Figs. 6, 8 jumps in phase

occur at frequencies corresponding to minima in the pressure amplitude. Although the parameter $(-\arg f_\infty/ka)$ varies continuously from zero as in the case of the rigid sphere, it does not appear that any direct physical interpretation should be applied to it concerning the apparent source of the echo. The representation should be regarded only as a convenient way of presenting the phase as a continuously varying function.

In order to determine the effect of distance of the sound source from the center of the sphere the function f in Eq. (18) was evaluated for a point source at various distances from a rigid, a free surface, and a brass sphere. The pressure amplitude $|f|$ multiplied by R is shown in Figs. 13 - 15, allowing a ready comparison with the solutions for a distant source $|f_\infty|$. In general it appears that f_∞ represents a satisfactory solution when the sound source is situated more than 10 radii from the center of the sphere.

4. Echo Pulse Forms

The most obvious general feature in the steady state solution for ordinary metals is the succession of peaks and minima in the pressure amplitude and it is of interest to determine how this affects the pulse form of the echo when the steady state solutions are used in the integral expression (23) for a distance source. The incident pulse form could be chosen arbitrarily. However in practice the incident sound is generally produced by making a transducer resonate over several cycles at a particular frequency. Mathematically the pressure variation which results at a point in the fluid can be represented as follows,

$$P_i(t) = 0 \qquad t < -\Delta t$$

$$= \exp(-i\omega_o t) \qquad -\Delta t < t < \Delta t \qquad (24)$$

$$= 0 \qquad t > \Delta t$$

where ω_o is the angular frequency of the transducer at resonance, and $2\Delta t$ is the duration of the pulse. The frequency spectrum $g(\omega)$ is given by the transform

$$g(\omega) = \frac{1}{2\pi} \int_{-\Delta t}^{\Delta t} \exp[i(\omega-\omega_o)t]\, dt$$

$$= \frac{2}{\pi} \sin[(\omega-\omega_o)\Delta t] / (\omega-\omega_o)$$

which in the non-dimensionalized system of Eq. (23) becomes

$$g(x) = \frac{2}{\pi} \sin[(x-x_o)\Delta\tau] / (x-x_o) \qquad (25)$$

where $x_o = \omega_o a/c$ and is referred to as the dominant frequency. By use of Eq. (25) and the previously derived values of the function f_∞ it is then possible to obtain the pulse form of the echo by numerically integrating Eq. (23).

The nature of the function g in Eq. (25) is shown in Figs. 16 - 18 for different pulse lengths $\Delta\tau$. The height of the main peak occurring at the dominant frequency is equal to $\Delta\tau$ and its "spread" varies inversely with $\Delta\tau$. If the function $|f_\infty|$ is momentarily idealized as consisting of a series of similar, equally spaced peaks, it would appear that the form of the echo depends mainly on the pulse length and on the location of the dominant frequency relative to the maxima and minima of the $|f_\infty|$.

Two extreme cases would then arise depending on whether the dominant frequency coincided with a maximum or with a minimum of $|f_\infty|$.

Using the data for Armco iron as shown in Figs. 5, 6 several echo pulse forms were computed for different lengths of the incident pulse and for dominant frequencies corresponding to values of x or ka at 24.5 and 25.5. The former frequency occurs at a peak of the pressure amplitude and the latter at a minimum. The range of integration over ka for the longer pulses was from 15 to 35, while for the short 5 cycle pulse, it extended from 10 to 40. The incident pulse did not therefore have a perfectly rectangular form. However in comparison to experimental pulse forms, it could be considered a satisfactory approximation. In addition the irregularities introduced by restricting the range of integration facilitated the recognition of certain features of the incident pulse in the echo. The calculated echoes are shown in Figs. 16 - 18. The time scale for the incident pulse is chosen with respect to the time of arrival of the mid-point of the pulse at the center of the sphere, whereas the scale for the echo is chosen with respect to the time of arrival back at the source. All pulses are shown travelling from right to left. It can be seen from these figures that the leading edge of the echo precedes that of the incident pulse by a time difference of 2 in each case. In addition the leading edge of the echo is of the same form as the leading edge of the incident pulse. These features indicate that the first part of the echo consists of a rigid body reflection from the region of the surface of the sphere adjacent to the sound source. The subsequent parts of the echo are affected by the vibrations of the sphere. In the case of the five cycle

pulse, the first echo is of identical form to the incident pulse, while the second echo is also of the same form, but inverted. Subsequent echoes diminish in amplitude and lose the characteristic features of the incident pulse. Whether the dominant frequency occurs at a minimum or a maximum of the function $|f_\infty|$ does not appear to make much difference to the form of the echo for the short five cycle pulse, but obviously it is important when the pulse is longer. The reason can be seen from the frequency spectra shown in Figs. 16-18. A change in ka of the order of 1 in the spectrum for the short pulse will not greatly affect the integral (23); however, this is not the case for the longer pulses. The differences in form of the echoes shown in Figs. 17, 18 are in fact quite distinctive. It seems moreover that the changes which occur when the dominant frequency is moved from a maximum of $|f_\infty|$ to a minimum, are characteristic of any ordinary metal. Figure 19 shows the echoes from a sphere of aluminum for the same type of incident pulse, where these results were obtained experimentally. With allowance for a change of scale and such effects as the response of the transducer, the differences in the echo resulting from a change in the dominant frequency are closely related to those shown in Figs. 16 - 18. The sphere in this case had a diameter of 5 inches and the change in dominant frequency was from 120 kc/sec to 123.5 kc/sec. This is equivalent to a change in ka of about 1, which according to Fig. 12 is the approximate distance between a peak and a minimum of the function $|f_\infty|$ for most metals including aluminum. Using the constants given above for water and aluminum, it is found that 120 kc/sec does not in fact coincide with a

pulse, the first echo is of identical form to the incident pulse, while the second echo is also of the same form, but inverted. Subsequent echoes diminish in amplitude and lose the characteristic features of the incident pulse. Whether the dominant frequency occurs at a minimum or a maximum of the function $|f_\infty|$ does not appear to make much difference to the form of the echo for the short five cycle pulse, but obviously it is important when the pulse is longer. The reason can be seen from the frequency spectra shown in Figs. 16-18. A change in ka of the order of 1 in the spectrum for the short pulse will not greatly affect the integral (23); however, this is not the case for the longer pulses. The differences in form of the echoes shown in Figs. 17, 18 are in fact quite distinctive. It seems moreover that the changes which occur when the dominant frequency is moved from a maximum of $|f_\infty|$ to a minimum, are characteristic of any ordinary metal. Figure 19 shows the echoes from a sphere of aluminum for the same type of incident pulse, where these results were obtained experimentally. With allowance for a change of scale and such effects as the response of the transducer, the differences in the echo resulting from a change in the dominant frequency are closely related to those shown in Figs. 16 - 18. The sphere in this case had a diameter of 5 inches and the change in dominant frequency was from 120 kc/sec to 123.5 kc/sec. This is equivalent to a change in ka of about 1, which according to Fig. 12 is the approximate distance between a peak and a minimum of the function $|f_\infty|$ for most metals including aluminum. Using the constants given above for water and aluminum, it is found that 120 kc/sec does not in fact coincide with a

peak of the steady state reflection function $|f_\infty|$. However this is not surprising since the values used referred to rolled aluminum. In addition if the frequency is to be expressed in terms of ka with any accuracy, it would be necessary to know the velocity of sound in water under the conditions of the experiment, and also the diameter of the sphere, to within less than 1%. Echoes were calculated for rolled aluminum at values of ka equal to 34.6 and 35.6 corresponding to frequencies of 122.3 kc/sec and 125.8 kc/sec, these values occurring at a maximum and a minimum respectively of the reflection function $|f_\infty|$. The pulse lengths $\Delta\tau$ were the same as those in Figs. 16 - 18. Similarly echoes were calculated for a brass sphere for frequencies at ka = 20.2 and 21.0. These echoes were found to have the same features. The leading edge was a rigid body reflection and the same kind of transition in pulse form occurred when the frequency and the pulse length were varied. With yellow brass the secondary echoes in the multiple echo forms had a bigger amplitude than the primary echo.

5. Discussion

Although this paper represents only a preliminary study, it may be worthwhile to consider the significance of the results in relation to the problem of using sonar echoes to obtain information about a target.

In the first place, it would seem that solid materials could be divided roughly into two groups, metallic flint-like substances and substances which are fairly pliant. This can be seen from the steady state solutions where the former is characterized by a succession of peaks and minima roughly the same distance apart, while the latter has sharper,

stronger peaks more closely spaced. Although all the echo forms which were calculated belong only to the first type, it is evident from the steady state solutions that there would be a difference in the general nature of echoes between the two groups. Hence there would exist the possibility of distinguishing for instance between a bare rock and a large fish.

Secondly, if the sonar target is known to be a homogeneous metallic sphere, then it is possible to determine its approximate radius by using data of the type shown in Fig. 19. The features of the transition between a peak and a minimum of the steady state reflection function $|f_\infty|$ for the long incident pulses is characteristic of most ordinary metals, as shown in the previous section. The transition is accomplished during a change in ka of the order of 1. Hence given an actual change in frequency in cycles per second, it is then possible to determine the radius a of the sphere. For example the transition in pulse form shown in Fig. 19 is achieved through a frequency change of 3.5 kc/sec corresponding to a change in ka of about 1 which therefore makes the radius of the sphere approximately 2.5 inches. In general however such an estimate would not be quite so accurate. It might also be possible to estimate the size of the sphere by varying the pulse length rather than the frequency, particularly if the dominant frequency occurs at a minimum of the reflection function $|f_\infty|$. However it would presumably be necessary to use both.

Finally, it has been shown[15] that there are significant differences in the steady state reflection function f_∞ for rigid bodies of

---

[15] R. Hickling; J.A.S.A., 30, 2, 137-139, Feb. 1958.

different shapes. Although these effects would be rendered more complicated by allowing for the vibrations of the solid material, it may be possible to use them to derive some information about the shape of a sonar target.

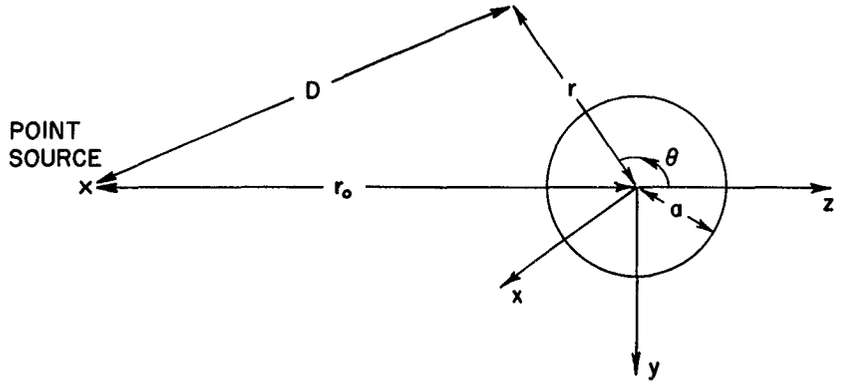

Fig. 1 Coordinate System

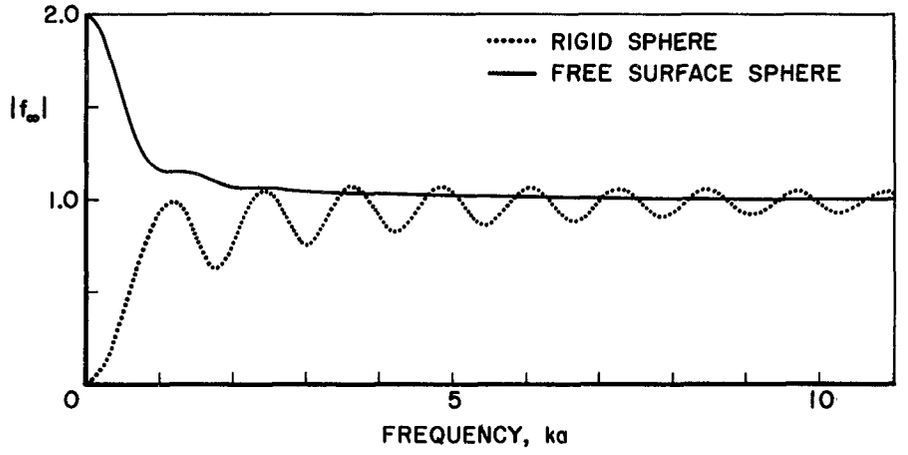

Fig. 2(a) The pressure amplitude as a function of frequency of the echo returned by rigid and free surface spheres to a distance source of continuous waves.

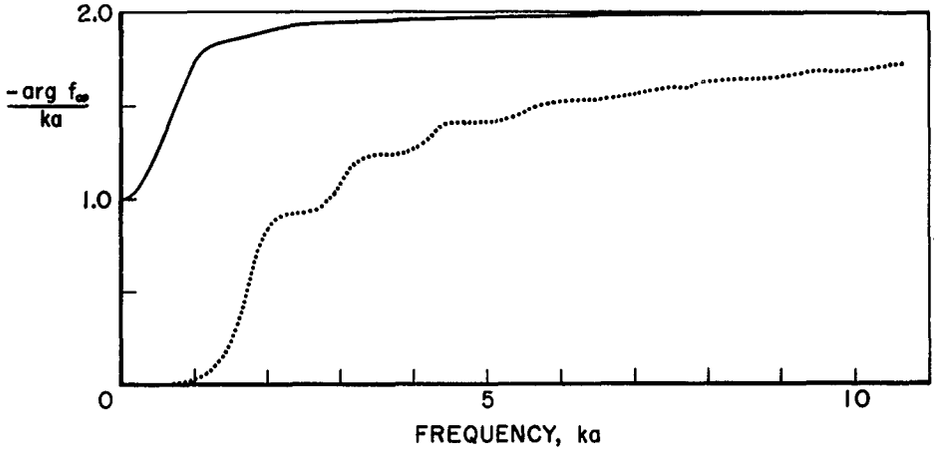

Fig. 2(b) The phase of the echo from rigid and free surface spheres as a function of frequency.

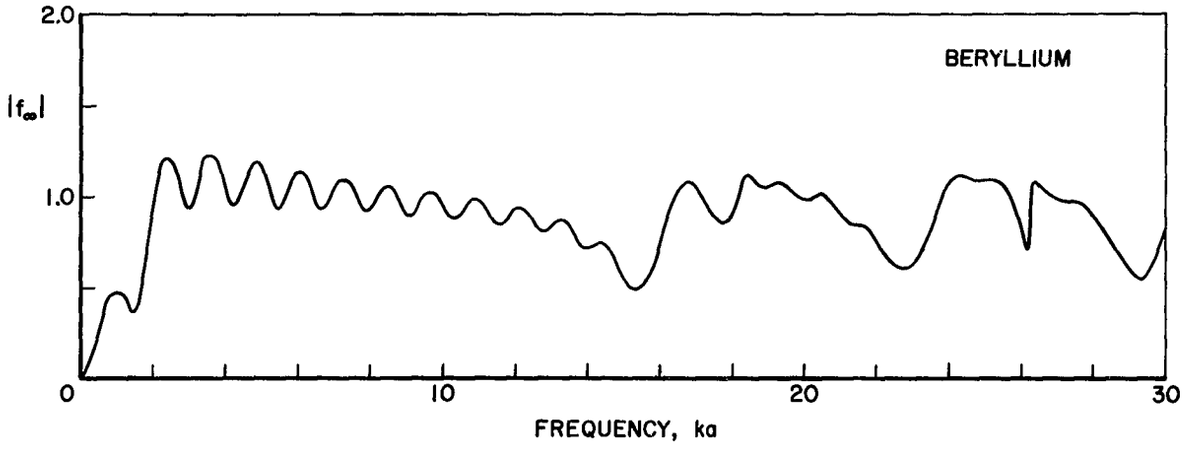

Fig. 3 The pressure amplitude as a function of frequency of the echo returned by a beryllium sphere to a distance source of continuous waves.

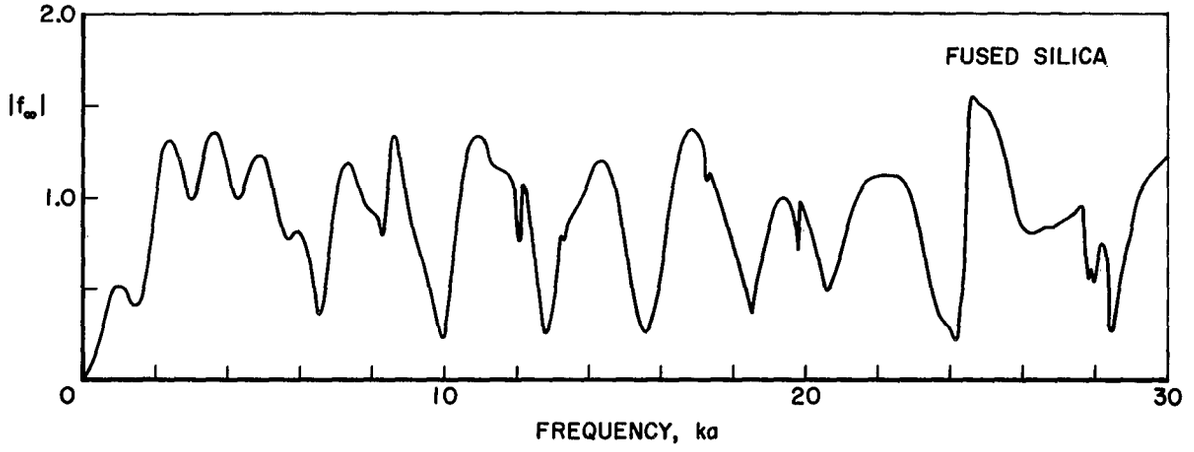

Fig. 4 The pressure amplitude as a function of frequency of the echo returned by a fused silica sphere to a distant source of continuous waves.

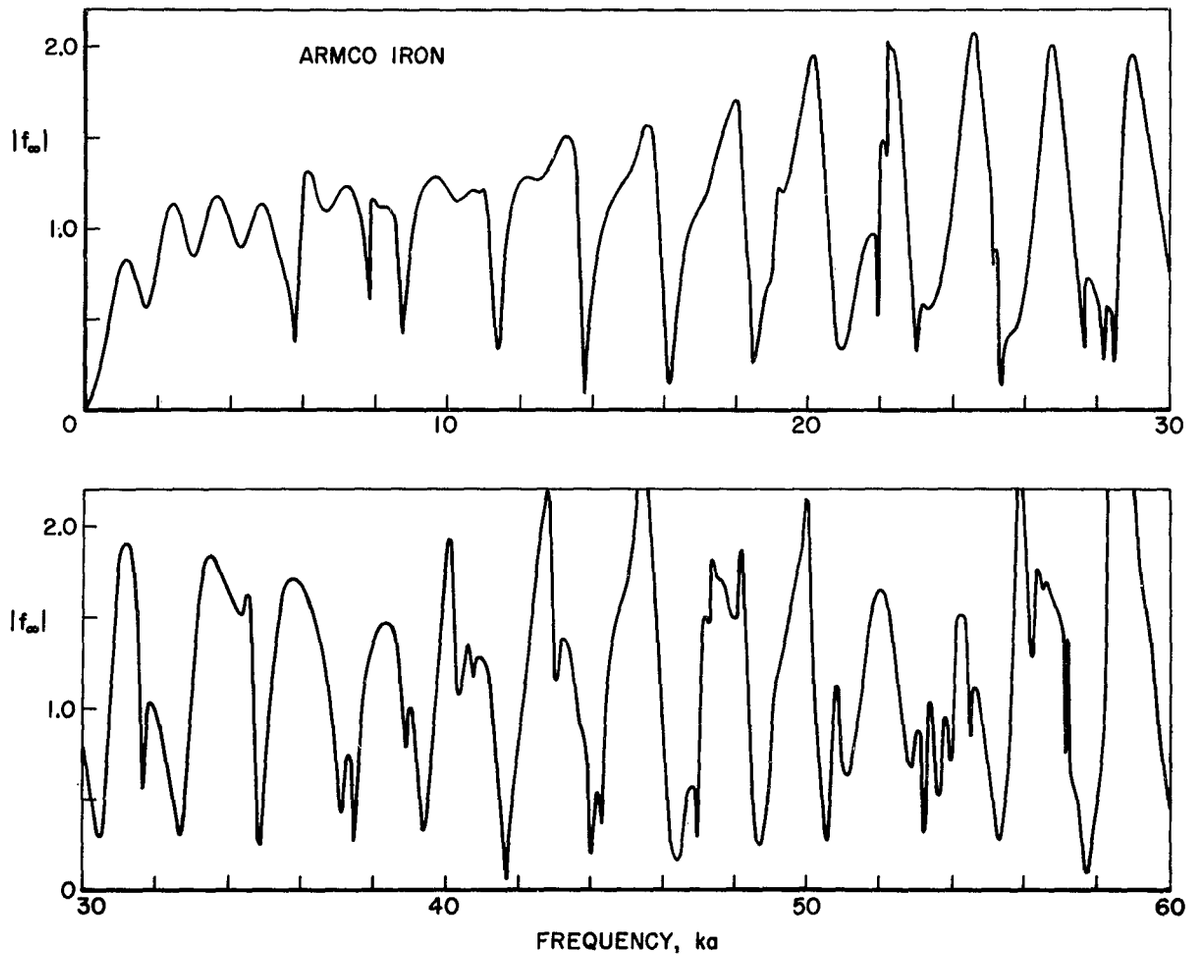

Fig. 5 The pressure amplitude as a function of frequency of the echo returned by a sphere of Armco iron to a distant source of continuous waves.

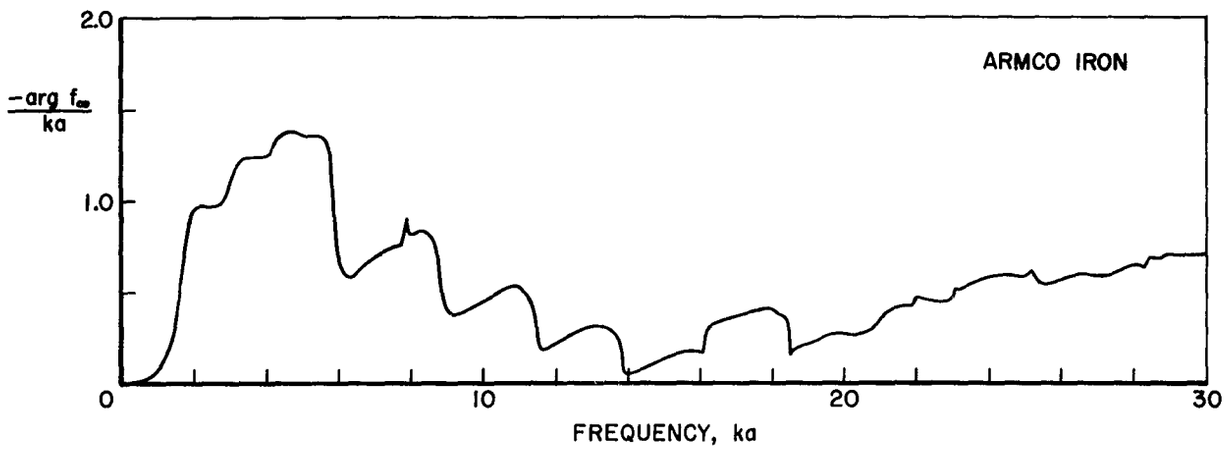

Fig. 6 The phase of the echo from the Armco iron sphere as a function of frequency.

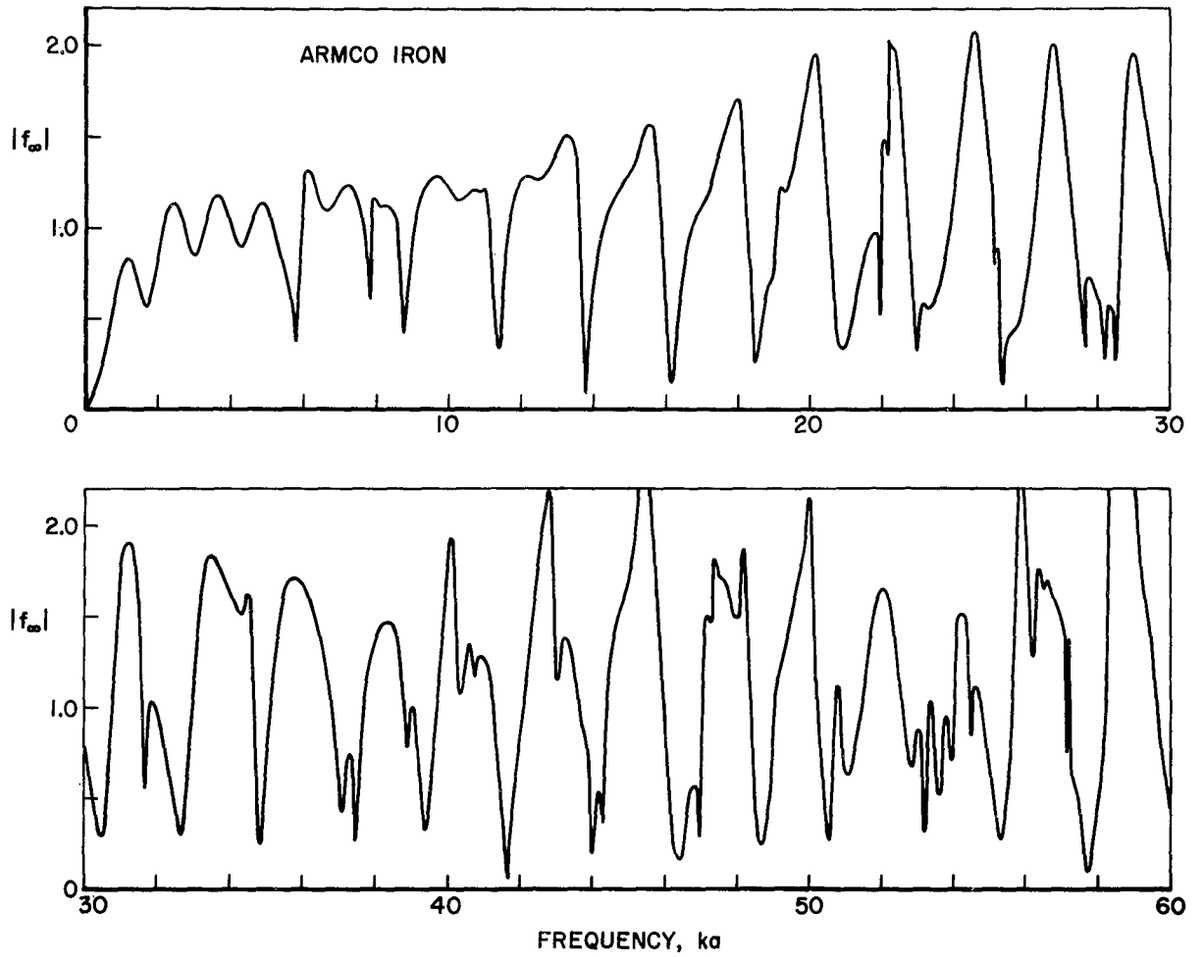

Fig. 5 The pressure amplitude as a function of frequency of the echo returned by a sphere of Armco iron to a distant source of continuous waves.

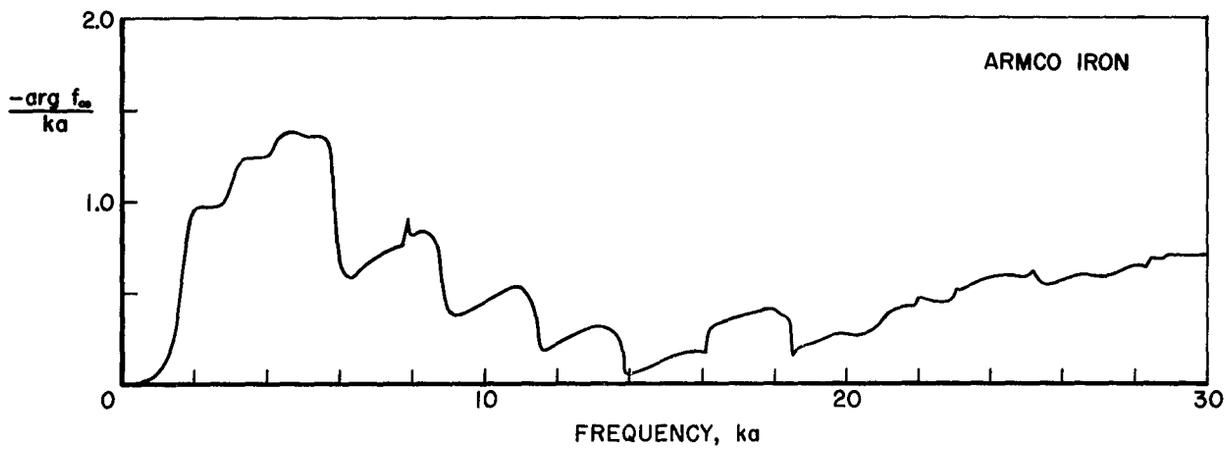

Fig. 6 The phase of the echo from the Armco iron sphere as a function of frequency.

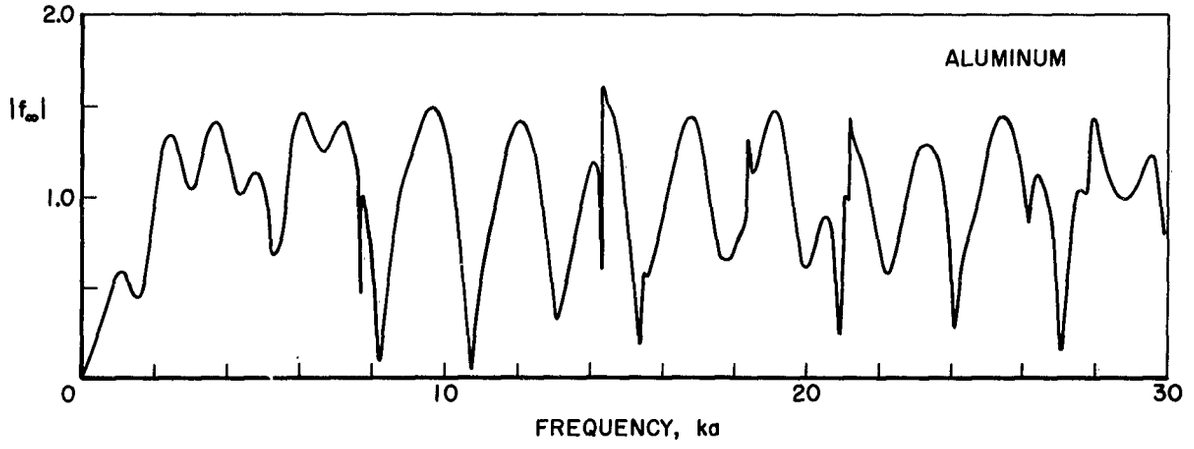

Fig. 7 The pressure amplitude as a function of frequency of the echo returned by an aluminum sphere to a distant source of continuous waves.

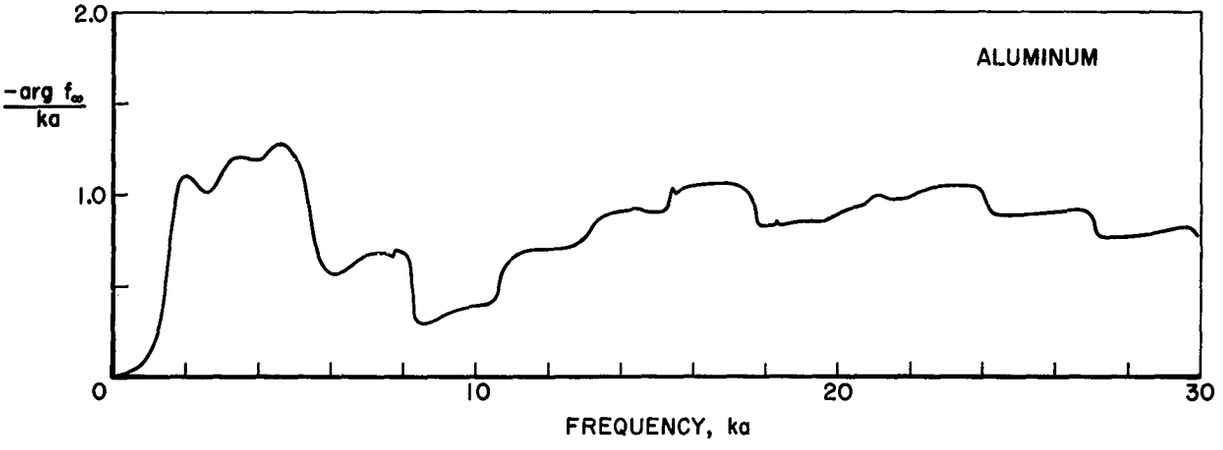

Fig. 8 The phase of the echo from the aluminum sphere as a function of frequency.

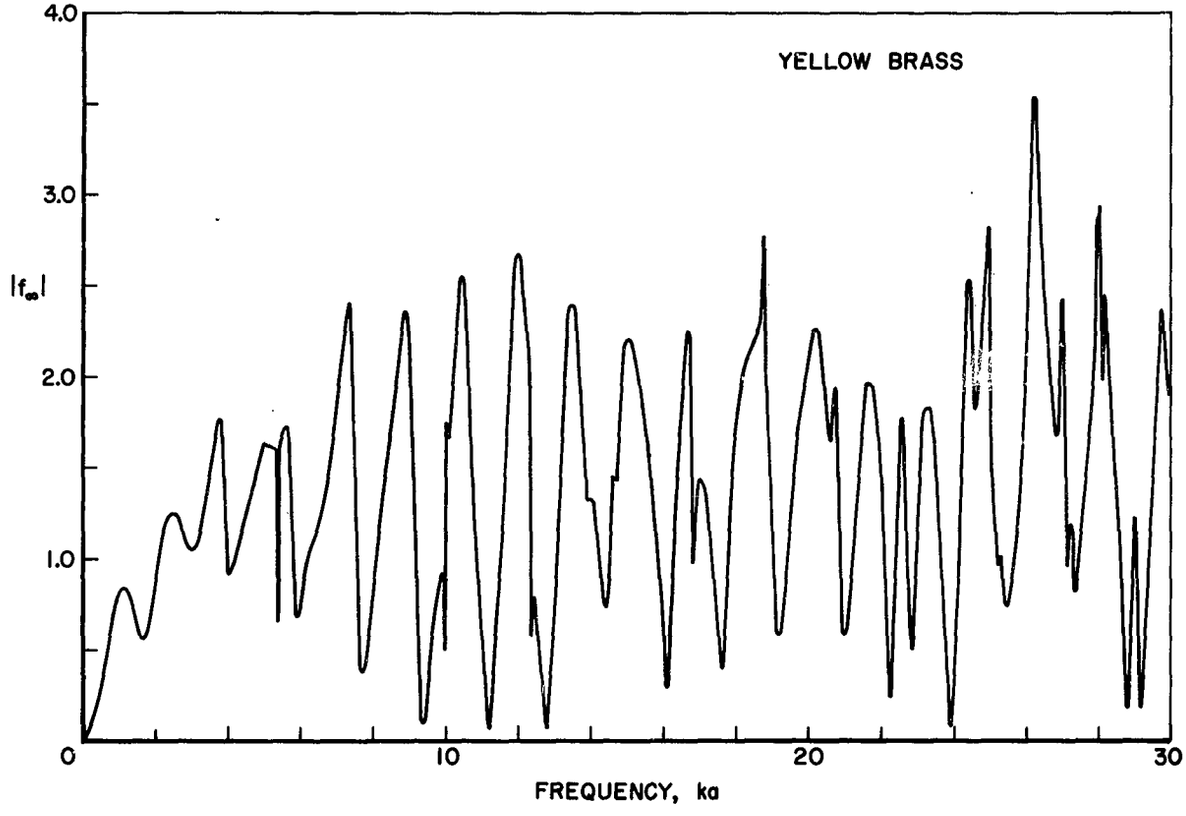

Fig. 9 The pressure amplitude as a function of frequency of the echo returned by a sphere of yellow brass to a distant source of continuous waves.

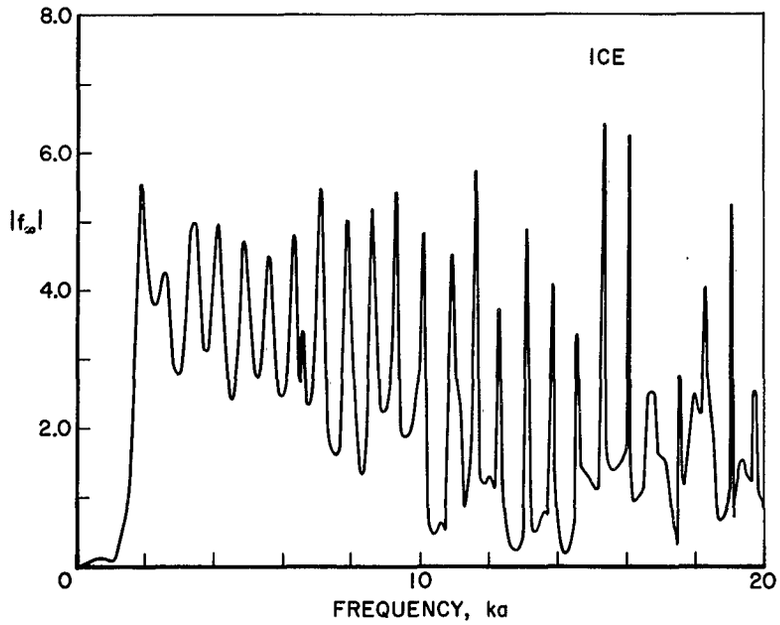

Fig. 10 The pressure amplitude as a function of frequency of the echo returned by an ice sphere to a distant source of continuous waves.

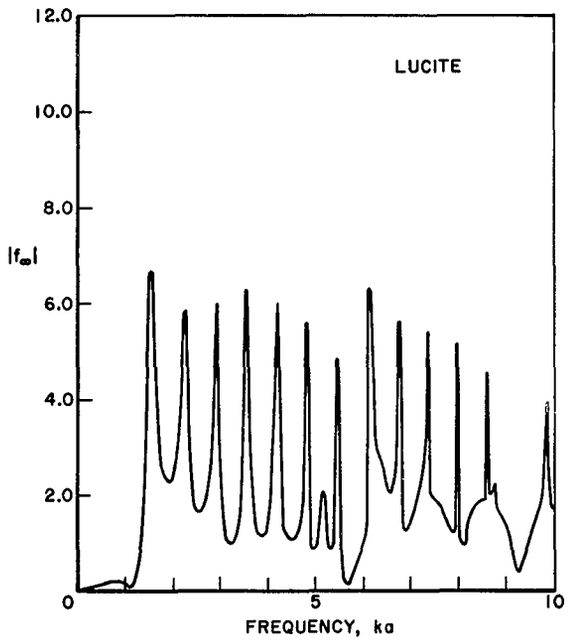

Fig. 11 The pressure amplitude as a function of frequency of the echo returned by a lucite sphere to a distant source of continuous waves.

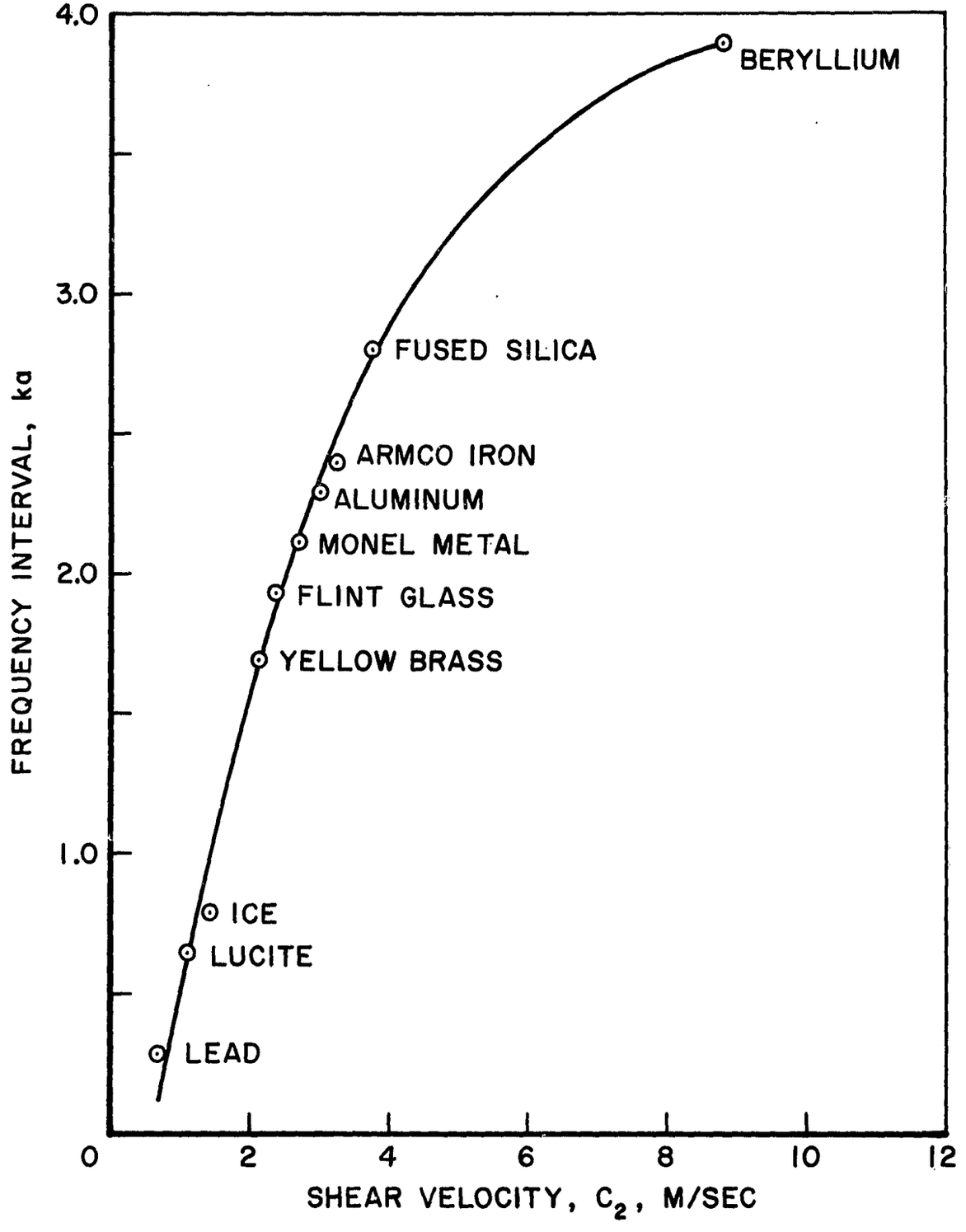

Fig. 12 Average interval in frequency between minima or between peaks in the pressure amplitude of the echo for different materials as a function of the shear velocity of the material.

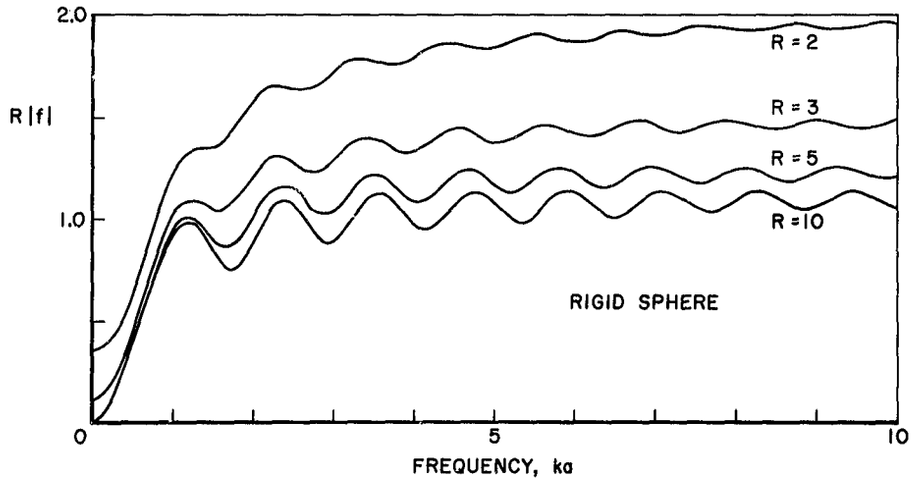

Fig. 13 The pressure amplitude as a function of frequency of the echo returned by a rigid sphere to a point source of continuous waves distance Ra from the center of the sphere.

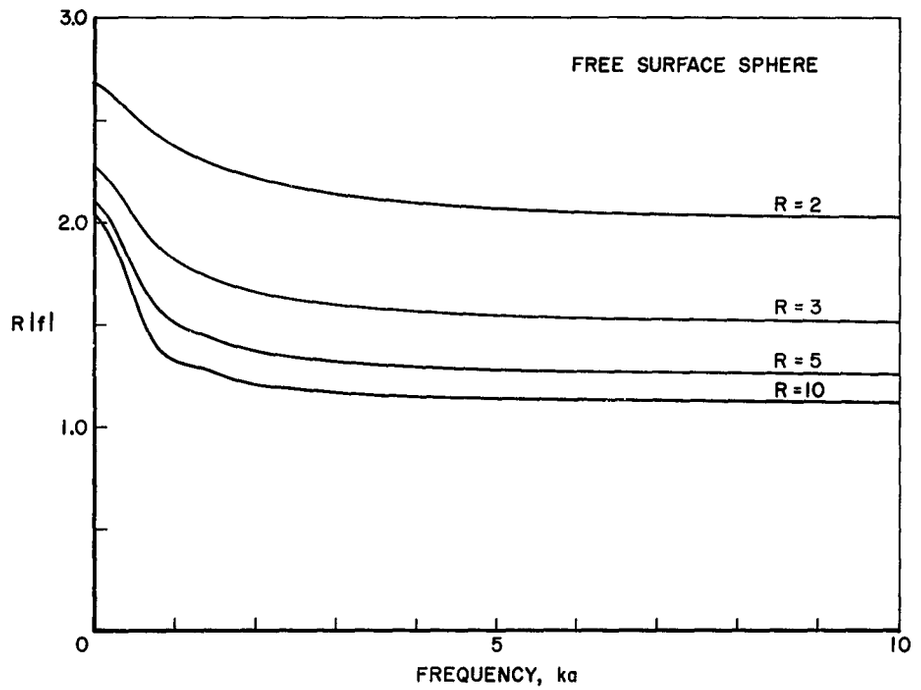

Fig. 14 The pressure amplitude as a function of frequency of the echo returned by a freee surface sphere to a point source of continuous waves distance Ra from the center of the sphere.

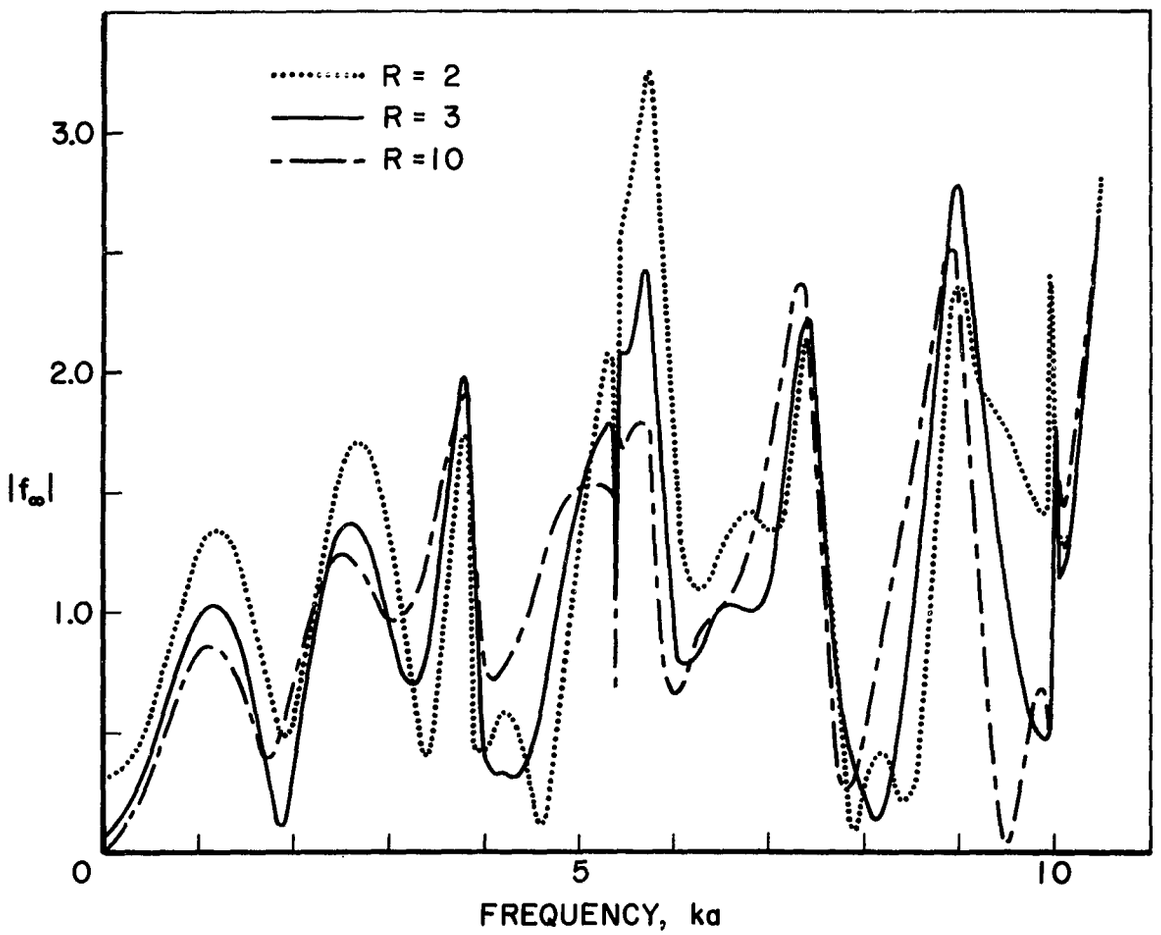

Fig. 15 The pressure amplitude as a function of frequency of the echo returned by a brass sphere to a point source of continuous waves distance Ra from the center of the sphere.

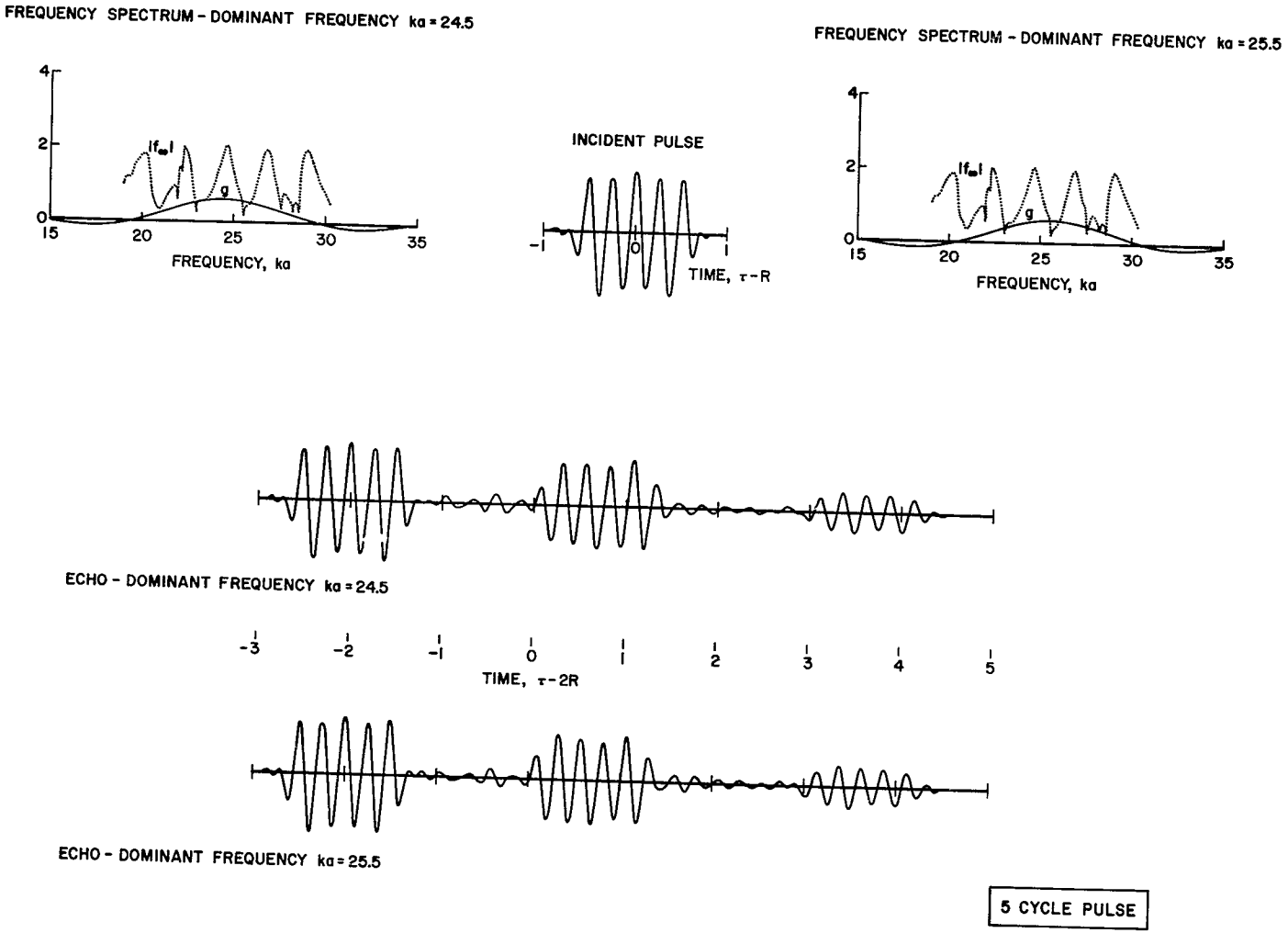

Fig. 16 Pulse forms of echoes returned by an Armco iron sphere for dominant frequencies at ka = 24.5 and 25.5 with an incident pulse of five cycles.

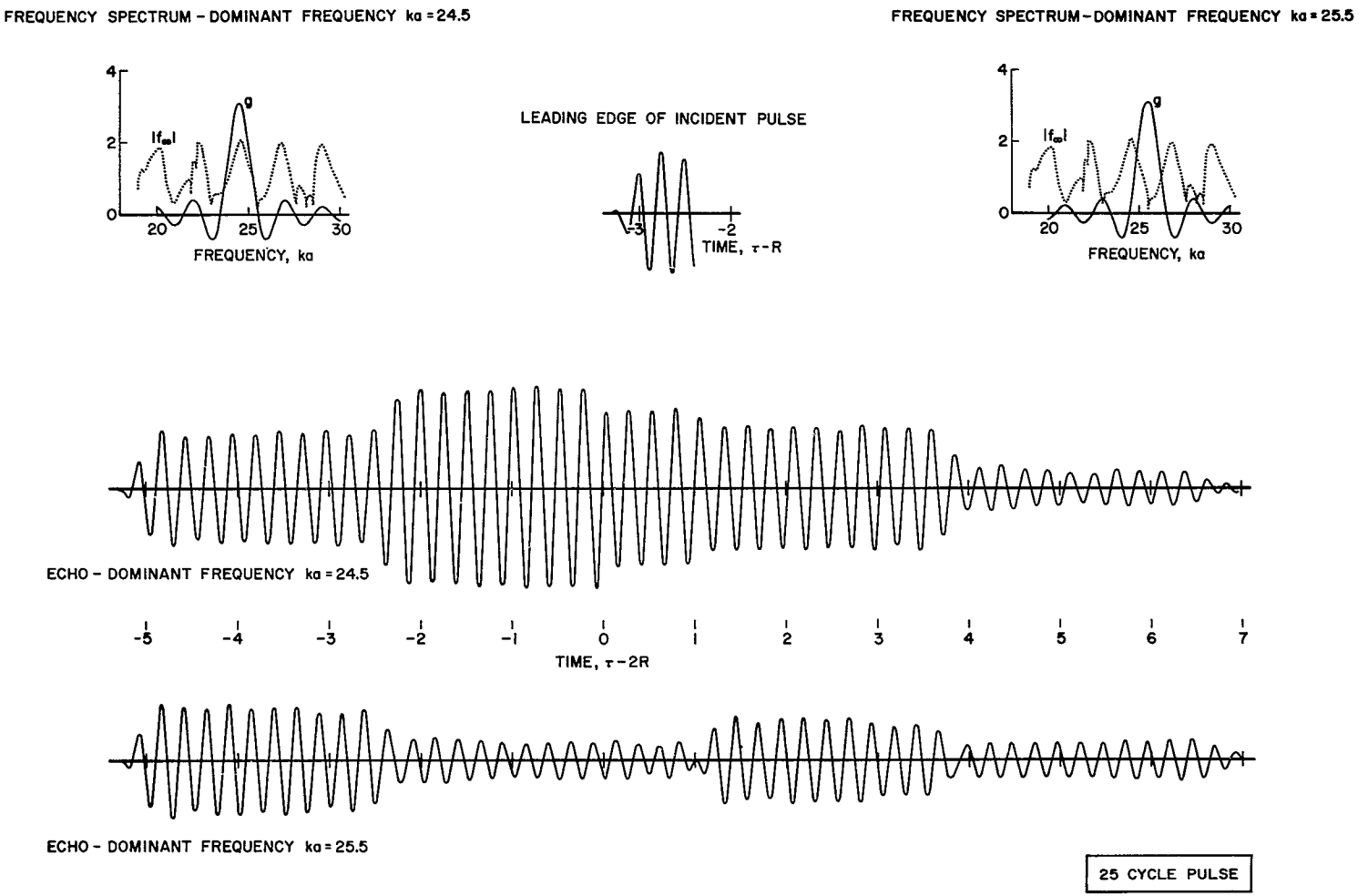

Fig. 17 Pulse forms of echoes returned by an Armco iron sphere for dominant frequencies at ka = 24.5 and 25.5 with an incident pulse of twenty-five cycles.

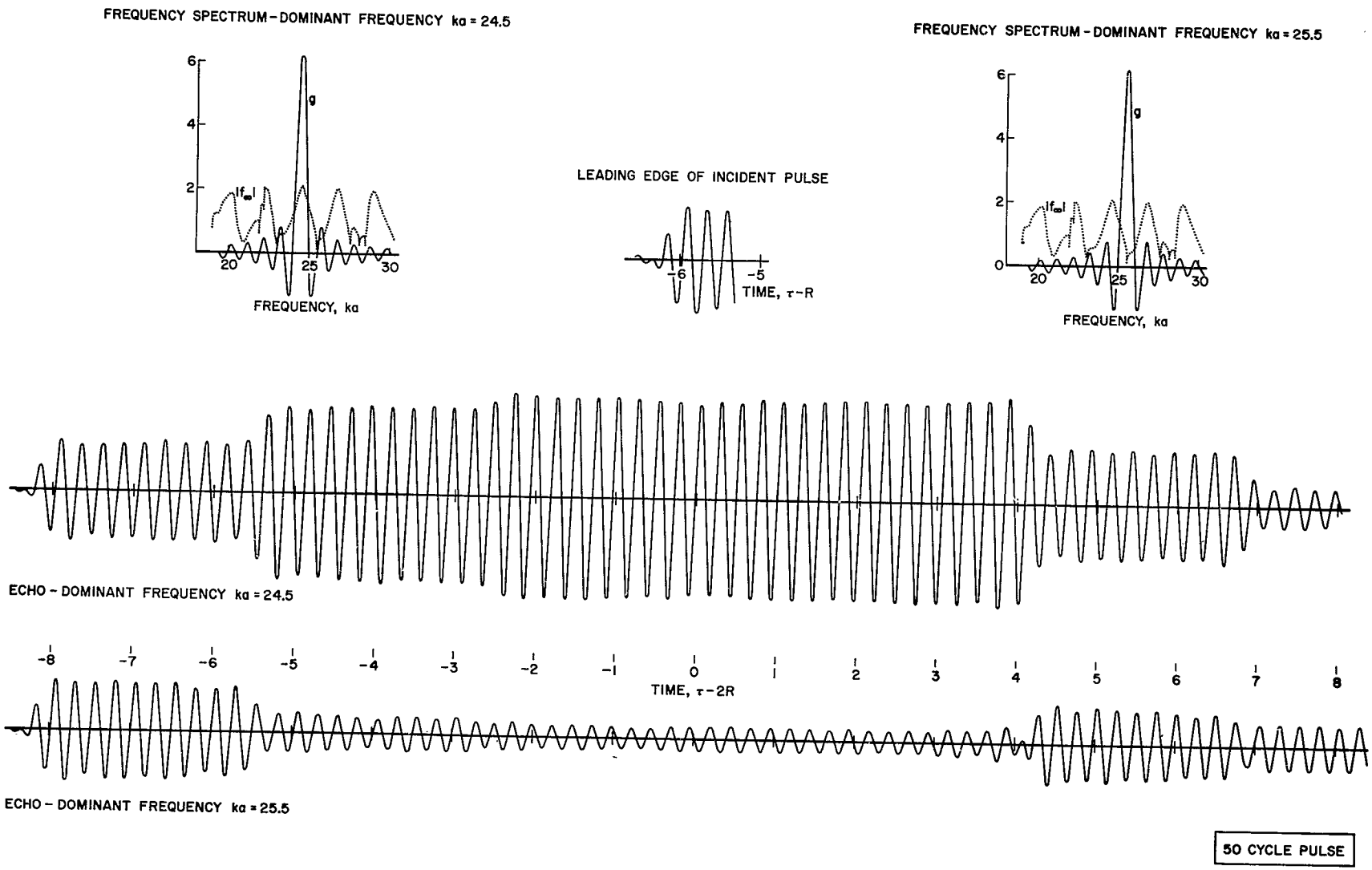

Fig. 18 Pulse forms of echoes returned by an Armco iron sphere for dominant frequencies at ka = 24.5 and 25.5 with an incident pulse of fifty cycles.

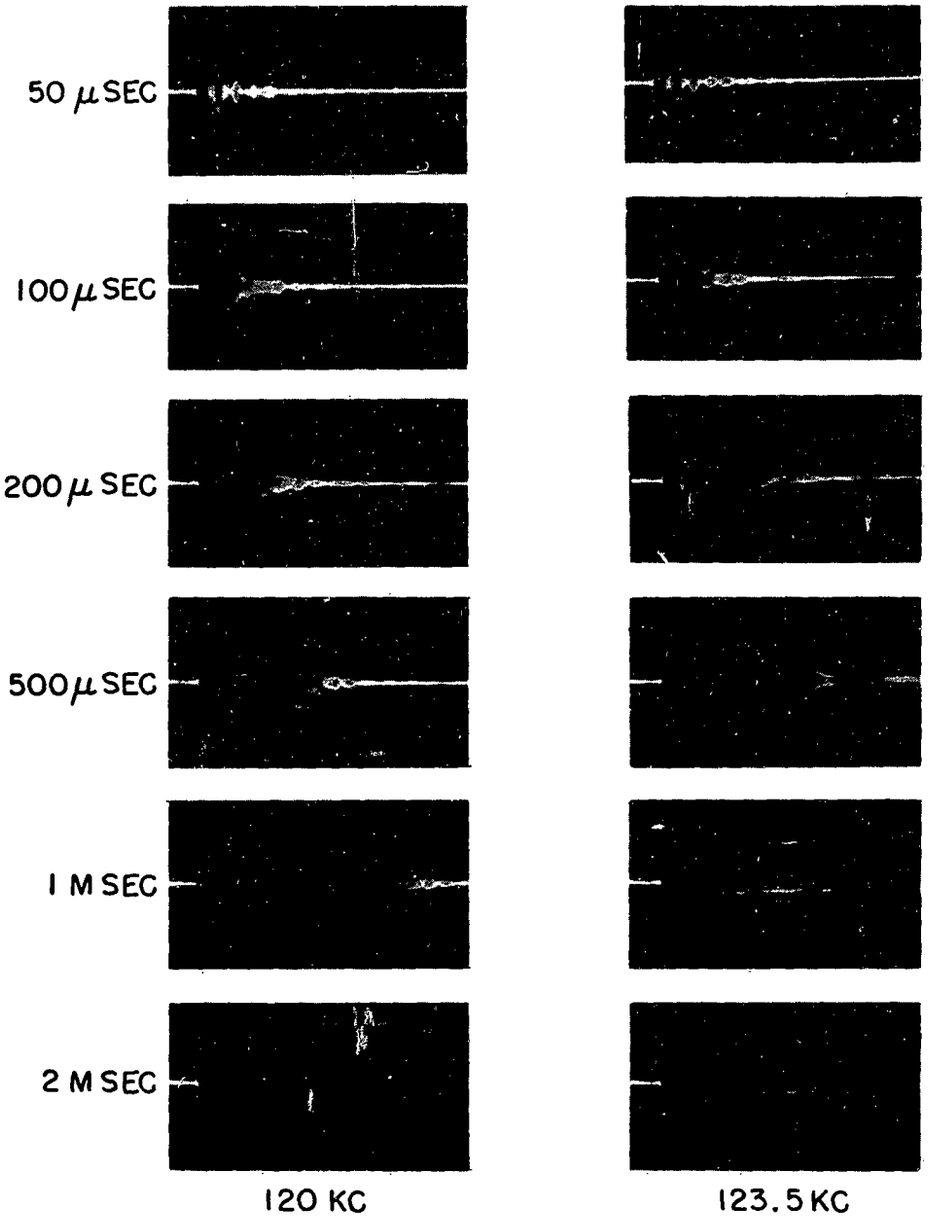

Fig. 19 Experimentally determined echo forms for a 5" diameter aluminum sphere for various incident pulse lengths. The sweep is 150 μ sec/cm.

DISTRIBUTION LIST FOR UNCLASSIFIED
REPORTS ON CAVITATION

Contract Nonr-220(28)
Single Copies Unless Otherwise Given

Chief of Naval Research
Navy Department
Washington 25, D. C.
Attn: Code 438 (3)
Code 463

Commanding Officer
Office of Naval Research
Branch Office
The John Crerar Library Bldg.
Chicago 1, Ill.

Commanding Officer
Office of Naval Research
Branch Office
346 Broadway
New York 13, N. Y.

Commanding Officer
Office of Naval Research
Branch Office
1030 E. Green Street
Pasadena, California

Commanding Officer
Office of Naval Research
Navy 100, Fleet Post Office
New York, N. Y. (25)

Director
Naval Research Laboratory
Washington 25, D.C.
Attn: Code 2021 (6)

Chief, Bureau of Aeronautics
Navy Department
Washington 25, D.C.
Attn: Research Division
Aero and Hydro Branch
(Code Ad-3)
Appl. Mech. Branch
(Code DE-3)

Commander
Naval Ordnance Test Station
Inyokern, China Lake, Calif.
Attn: Technical Library

Commander
Naval Ordnance Test Station
3202 E. Foothill Blvd.
Pasadena, California
Attn: Head, Underwater Ord.
Head, Research Div.
Pasadena Annex Library

Chief, Bureau of Weapons
Navy Department
Washington 25, D.C.
Attn: Asst. Chief for Research (Code Re)
Systems Director, Underwater Ord. (Code Rexc)
Armor, Bomb, Projectile, Rocket, Guided Missile Warhead and Ballistics Branch (Code Re3)
Torpedo Branch (Code Re6)
Research and Components Section (Code Re6a)
Mine Branch (Code Re7)

Chief, Bureau of Ships
Navy Department
Washington 25, D. C.
Attn: Research and Development (Code 300)
Ship Design (Code 410)
Preliminary Design and Ship Protection (Code 420)
Scientific, Structural and Hydrodynamics (Code 442)
Submarine (Code 525)
Propellers and Shafting (Code 554)

Chief, Bureau of Yards and Docks, Navy Department
Washington 25, D.C.
Attn: Research Division

Commanding Officer and Dir.
David Taylor Model Basin
Washington 7, D.C.
Attn: Hydromechanics Lab.
Seaworthiness and Fluid Dynamics Div.
Library

Commanding Officer
Naval Ordnance Laboratory
White Oak, Maryland
Attn: Underwater Ordnance Dept.

Commanding Officer
Naval Underwater Ordnance Station
Newport, Rhode Island

Director
Underwater Sound Laboratory
Fort Trumbull
New London, Conn.

Library
U. S. Naval Postgraduate School
Monterey, California

Executive Secretary Research and Development Board
Department of Defense
The Pentagon
Washington 25, D. C.

Chairman
Underseas Warfare Committee
National Research Council
2101 Constitution Avenue
Washington 25, D.C.

Dr. J. H. McMillen
National Science Foundation
1520 H Street, N. W.
Washington, D.C.

Director
National Bureau of Standards
Washington 25, D. C.
Attn: Fluid Mech. Section

Dr. G. H. Keulegan
National Hydraulic Laboratory
National Bureau of Standards
Washington 25, D. C.

Director of Research
National Aeronautics and
Space Administration
1512 H Street, N.W.
Washington 25, D.C.

Director
Langley Aeronautical Lab.
National Aeronautics and Space
Admin.
Langley Field, Virginia

Mr. J. B. Parkinson
Langley Aeronautical Lab.
National Aeronautics and
Space Administration
Langley Field, Virginia

Commander
Air Research and Develop-
ment Command
P. O. Box 1395
Baltimore 18, Maryland
Attn: Fluid Mechanics Div.

Director
Waterways Experiment Sta.
Box 631
Vicksburg, Mississippi

Beach Erosion Board
U.S. Army Corps of Engineers
Washington 25, D.C.

Office of Ordnance Research
Department of the Army
Washington 25, D.C.

Office of the Chief of Engineers
Department of the Army
Gravelly Point
Washington 25, D. C.

Commissioner
Bureau of Reclamation
Washington 25, D.C.

Director
Oak Ridge National Lab.
P. O. Box P
Oak Ridge, Tenn.

Sandia Corporation Library
Sandia Base
Albuquerque, New Mexico

Professor Carl Eckart
Scripps Institute of
Oceanography
La Jolla, California

Documents Service Center
Armed Services Technical
Information Agency
Arlington Hall Station
Arlington 12, Virginia (10)

Mr. A. B. Needham
Research Director
Minneapolis Mining
Research Center
Minneapolis 17, Minn.

Office of Technical Services
Department of Commerce
Washington 25, D.C.

Polytechnic Inst. of Brooklyn
Department of Aeronautical
Engineering and Applied Mech.
99 Livingston Street
Brooklyn 1, New York
Attn: Prof. H. Reissner

Division of Applied Mathematics
Brown University
Providence 12, Rhode Island

California Institute of Technology
Pasadena, California
Attn: Professor A. J. Acosta
Professor A. Hollander
Professor C.B. Millikan
Professor M.S. Plesset
Professor V.A. Vanoni
Professor T.Y. Wu

University of California
Department of Engineering
Berkeley 4, California
Attn: Professor H.A. Einstein
Professor H.A. Schade
Professor J.V. Wehausen

Case Institute of Technology
Dept. of Mechanical Engineering
Cleveland, Ohio
Attn: Professor G. Kuerti

Cornell University
Grad. School of
Aeronautical Eng.
Ithaca, New York
Attn: Prof. W.R. Sears

Harvard University
Cambridge 38, Mass.
Attn: G. Birkhoff, Dept.
of Mathematics
G. Carrier, Div. of
Eng. and Appl. Physics

University of Illinois
Dept. of Theoretical and
Applied Mechanics
College of Engineering
Urbana, Illinois
Attn: Dr. J.M. Robertson

State University of Iowa
Iowa Institute of Hydraulic
Research
Iowa City, Iowa
Attn: Dr. Hunter Rouse

University of Maryland
Inst. for Fluid Dynamics
and Applied Math.
College Park, Maryland
Attn: Prof. M.H. Martin
Prof. J.R. Weske

Massachusetts Institute
of Technology
Cambridge 39, Mass.
Attn: Prof. W.M. Rohsenow
Dept. Mech. Engr.
Prof. A.T. Ippen
Hydro. Lab.

Michigan State College
Hydraulics Laboratory
East Lansing, Mich.
Attn: Prof. H.R. Henry

University of Michigan
Ann Arbor, Michigan
Attn: Director, Engineer-
ing Institute
Prof. V.L. Streeter,
Civil Eng. Dept.

University of Minnesota
St. Anthony Falls Hyd. Lab.
Minneapolis 14, Minn.
Att: Dr. L.G. Straub

New York University
Inst. of Mathematical Sciences
25 Waverly Place
New York 3, New York
Attn: Prof. R. Courant

University of Notre Dame
College of Engineering
Notre Dame, Indiana
Attn: Dean K.E. Schoenherr

Pennsylvania State University
Ordnance Research Laboratory
University Park, Pennsylvania
Attn: Prof. G. F. Wislicenus

Dr. J. Kotik
Technical Research Group
2 Aerial Way
Syosset, New York

Professor H. Cohen
IBM Research Center
P.O. Box 218
Yorktown Heights, New York

Stanford University
Stanford, California
Attn: Prof. D. Gilbarg, Dept. of Mathematics
Prof. L.I. Schoff, Dept. of Physics
Prof. J.K. Vennard, Dept. of Civil Eng.

Stevens Institute of Technology
Experimental Towing Tank
711 Hudson Street
Hoboken, New Jersey

Worcester Polytechnic Institute
Alden Hydraulic Laboratory
Worcester, Mass.
Attn: Prof. J.L. Hooper

Dr. Th. von Karman
1051 S. Marengo Street
Pasadena, California

Aerojet General Corporation
6352 N. Irwindale Avenue
Azusa, California
Attn: Mr. C.A. Gongwer

Dr. J. J. Stoker
New York University
Inst. of Mathematical Sciences
25 Waverly Place
New York 3, New York

Prof. C.C. Lin
Dept. of Mathematics
Massachusetts Inst. of Tech.
Cambridge 39, Mass.

Dr. Columbus Iselin
Woods Hole Oceanographic Inst.
Woods Hole, Mass.

Dr. A.B. Kinzel, Pres.
Union Carbide and Carbon Research Laboratories, Inc.
30 E. 42nd Street
New York, N. Y.

Dr. F. E. Fox
Catholic University
Washington 17, D.C.

Dr. Immanuel Estermann
Office of Naval Research
Code 419
Navy Department
Washington 25, D.C.

Goodyear Aircraft Corporation
Akron 15, Ohio
Attn: Security Officer

Dr. F. V. Hunt
Director, Acoustics Research Laboratory
Harvard University
Cambridge, Mass.

Prof. Robert Leonard
Dept. of Physics
University of California at Los Angeles
West Los Angeles, California

Technical Librarian
AVCO Manufacturing Corp.
2385 Revere Beach Parkway
Everett 49, Mass.

Dr. L. Landweber
Iowa Inst. of Hydraulic Research
State University of Iowa
Iowa City, Iowa

Dr. M. L. Ghai
Supervisor
Heat Transfer/Fluid Mechanics
Rocket Engine-Applied Research
Building 600
Aircraft Gas Turbine Div.
General Electric Co.
Cincinnati 15, Ohio

Dr. W. W. Clauson
Rose Poly. Inst.
R.R. No. 5
Terre Haute, Indiana

Mr. Kurt Berman
Rocket Engine Section
Aircraft Gas Turbine
Development Dept.
Malta Test Station
Ballston Spa, New York

Officer in Charge
MWDP Contract Supervisory Staff
SACLANT ASW Research Center
APO 19, New York, N.Y.

Hydronautics, Inc.
200 Monroe Street
Rockville, Maryland
Attn: Mr. Phillip Eisenberg
Mr. Marshall P. Tulin

Commanding Officer and Director
U.S. Naval Civil Eng. Lab.
Port Hueneme, California
Attn: Code L54

Dr. H. L. Uppal, Director
Irrigation and Power Research Institute
Punjab, Amritsar, India

Prof. Taizo Hayashi, Director
Hydraulics Laboratory
Chuo University
1, 1-chome, Koishikawa-mati
Bunkyo-ku, Tokyo, Japan

Prof. J. E. Cermak
Department of Civil Engineering
Colorado State University
Fort Collins, Colorado

Mr. John P. Herling
Order Librarian
Engineering Societies Library
United Engineering Trustees, Inc.
29 West 39th Street
New York 18, N. Y.

Mr. R. W. Kermeen
Dept. 8173, Bldg. 181N
Lockheed Missile and Space Company
P. O. Box 504
Sunnyvale, California

Material Laboratory Library
Building 291, Code 912B
New York Naval Shipyard
Brooklyn 1, New York

Professor Frederick G. Hammitt
Nuclear Engineering Department
The University of Michigan
Research Institute
Ann Arbor, Michigan

Commanding Officer
NROTC and Naval Administrative Unit
Massachusetts Institute of Technology
Cambridge 39, Mass.

Commanding Officer and Director
U.S. Navy Mine Defense Laboratory
Panama City, Florida